

Excellence in Chemistry Research



Announcing our new flagship journal

- Gold Open Access
- Publishing charges waived
- Preprints welcome
- Edited by active scientists



Meet the Editors of ChemistryEurope





Luisa De Cola Università degli Studi di Milano Statale, Italy



Ive Hermans
University of
Wisconsin-Madison, USA



Ken Tanaka Tokyo Institute of Technology, Japan

Check for updates



www.chemeurj.org

Metal-Mediated Directional Capping of Rod-Packing Metal-Organic Frameworks

Anh N. Hong,^[a] Diana Luong,^[a] Mohammed Alghamdi,^[b] Wei-Cheng Liao,^[b] Weiyi Zhang,^[c] Emily Kusumoputro,^[a] Yichong Chen,^[a] P. Alex Greaney,^[c] Yongtao Cui,^[b] Jing Shi,^[b] Xianhui Bu,^[d] Boniface P. T. Fokwa,*^[a] and Pingyun Feng*^[a]

Abstract: Two new rod-packing metal-organic frameworks (RPMOF) are constructed by regulating the in situ formation of the capping agent. In CPM-s7, carboxylate linkers extend 1D manganese-oxide chains in four additional directions, forming 3D RPMOF. The substitution of Mn²⁺ with a stronger Lewis acidic Co²⁺, leads to an acceleration of the hydrolysis-prone sulfonate linker, resulting in presence of sulfate ions to

reduce two out of the four carboxylate-extending directions, and thus forming a new 2D rod-packing CPM-s8. Density functional theory calculations and magnetization measurements reveal ferrimagnetic ordering of CPM-s8, signifying the potential of exploring 2D RPMOF for effective low-dimensional magnetic materials.

Introduction

Of great interest to researchers in the field of metal–organic framework (MOF) is the capability to design and construct novel intriguing structures of varied dimensions, pore metrics, and functionalities.^[1] At the core, MOF design relies heavily upon its secondary building unit (SBU), a module embedded with inherent properties that allow assembled materials to exhibit exceptional performances.^[2]

Among different secondary building units (SBU) employed in 3D-MOF design, the infinite rod-shaped SBU is of particular interest. [3] Compared to 3D MOFs with discrete SBUs, 3D rod-packing MOFs (RPMOF) easily overcome the possibility of interpenetration, a phenomenon that drastically reduces porosity. [4] Rod-shaped SBU exhibits much higher open-metal-site density (e.g., MOF-74-Ni, with inorganic helical chains, has one of the highest metal density at approximately

7.74 mmol cm⁻³).^[5] Without long organic linker connecting different metal nodes, efficiency of transporting electronic information is boosted dramatically.^[6] These outstanding features have allowed many 3D RPMOFs to have great potential in a variety of applications.^[7]

Compared to 3D RPMOFs, the self-assembly of 2D RPMOFs are less known. [8] Construction of 2D RPMOF requires a synthetic environment that simultaneously promotes the growth of inorganic unit along one dimension, and caps organic linker along one of the two remaining dimensions, which poses a significant challenge. But given the importance inorganic rod-packing chains, it is of high interest to synthesize and explore properties unique to 2D RPMOF materials.

Herein, we report a metal-mediated design strategy to control dimensions of RPMOFs. Synthetic exploration of manganese salt and a polyfunctional linker, 4,8-disulfo-napthalene-dicarboxylic acid (H₄dsndc) resulted in the assembly of a 3D RPMOF, [Mn₃(dsndc)(HCOO)₂(H₂O)₃(EtOH)]·H₂O (CPM-s7). From structural analysis of CPM-s7, we predicted the possibility of introducing a capping agent to inhibit growth of organic linkers in two directions (Figure 1). We took advantage of sulfonic acid



- [b] M. Alghamdi, W.-C. Liao, Prof. Y. Cui, Prof. J. Shi Department of Physics and Astronomy University of California, Riverside 900 University Avenue, Riverside, CA 92521 (USA)
- [c] W. Zhang, Prof. P. A. Greaney Department of Materials Science and Engineering University of California, Riverside 900 University Avenue, Riverside, CA 92521 (USA)
- [d] Prof. X. Bu

 Department of Chemistry and Biochemistry

 California State University Long Beach

 1250 Bellflower Boulevard, Long Beach, CA 90840 (USA)
- Supporting information for this article is available on the WWW under https://doi.org/10.1002/chem.202201576

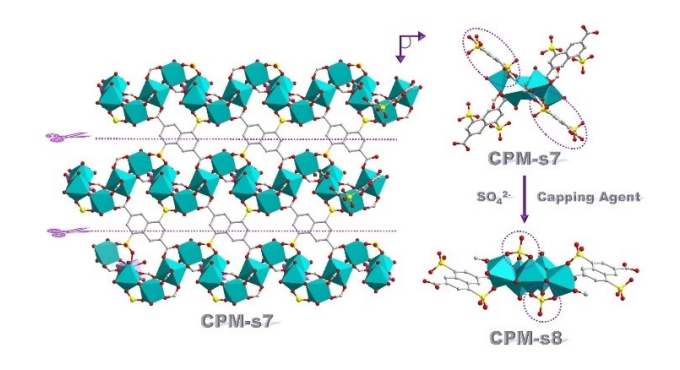


Figure 1. Transformation of 3D CPM-s7 to 2D CPM-s8 through in situ formation of $SO_4^{\ 2^-}$ capping agent.

Chemistry Europe

European Chemical Societies Publishing

hydrolysis, which is generally accelerated at elevated temperature and/or acidity, to in situ generate sulfate capping agent. The presence of sulfate reduces the organic-extension of CPM-s7 by two directions, resulting in a novel 2D RPMOF, $[\text{Co}_5(\text{OH})_2(\text{SO}_4)_2(\text{HCOO})_2(\text{dsndc})(\text{DMF})_2(\text{H}_2\text{O})_2]$ (NH₂(CH₃)₂)₂(H₂O)₄ (CPM-s8). More interestingly, the presence of metal-oxide chain allows for long-range magnetic ordering at specified temperature, as predicted by density functional theory calculations and confirmed by magnetization measurements.

Results and Discussion

Crystal structure: CPM-s7 crystallizes in P-1 space group, with asymmetric unit consisting of four unique Mn²⁺, one dsndc⁴⁻, two HCOO-, one EtOH, and five H₂O molecules, where Mn(1) and Mn(4) reside in symmetry sites, and formate ions originate from hydrolysis of DMF. As shown in Figure 2b, Mn(1) and Mn(2) are bridged by six carboxylates into linear trimers. The two carboxylate ends of dsndc⁴⁻ link these trimers into 2D square layers stacked in ABAB conformation. These layers are further linked into 3D RPMOF framework by connecting two pendant formates of neighboring metal trimer with Mn(3) and sulfonate group of dsndc4- along b-axis to apex of trimer (Figure S1). Along ac-plane, pendant formate groups from trimer and sulfonate groups from dsndc⁴⁻ (parallel to c-axis) further trap Mn(4) ions, and thus removing pore opening along this direction. The 3D RPMOF has 1D rectangular channel with width ~5.7 Å (measured from oxygens of sulfonate groups).

CPM-s7 could also be viewed as wavy manganese chains linked by Mn(HCOO⁻)₂ and dsndc⁴⁻ into 2D layers (along ac plane). These layers are further pillared by remaining dsndc⁴⁻ groups into 3D framework. Thus, an introduction of capping agents could block the growth of dsndc⁴⁻ pillars, leading to construction of 2D RPMOF. Since both amide and sulfonate groups are prone to hydrolysis in elevated temperature, we hypothesized that the synthetic environment of CPM-s7, which favored hydrolysis of DMF and addition of formate into final framework, could also be tuned to favor hydrolysis of sulfonate group and addition of sulfate capping agent into final framework.

Hydrolysis reactions are well known to be accelerated under acidic conditions. With each transition metal-salt offering different Lewis acid strengths, introduction of a different metal could shift equilibrium condition slightly towards formation of sulfate capping agent. To validate our hypothesis, we substituted $\text{MnCl}_2 \cdot 4\text{H}_2\text{O}$ with stronger Lewis acid transition metal salts.

The hydrolysis DMF and H_4 dsndc to produce formate and sulfate, combined with evaporation of EtOH and H_2 O, resulted in the self-assembly of Co^{2+} and linkers into a novel 2D PRMOF. Similar to CPM-s7, single crystal X-ray diffraction of CPM-s8 also shows crystallization of material in P-1 space group. The composition of CPM-s8, however, differs dramatically from CPM-s7. Asymmetric unit of CPM-s8 contains three unique Co atoms (one of which resides on a symmetry site), half $dsndc^{4-}$, one OH^- , two $HCOO^-$, one SO_4^{2-} , one $(H_2N(CH_3)_2)^+$, one DMF and three H_2O molecules. All Co^{2+} atoms in this MOF are octahedrally coordinated with slight distortions. The Co-O

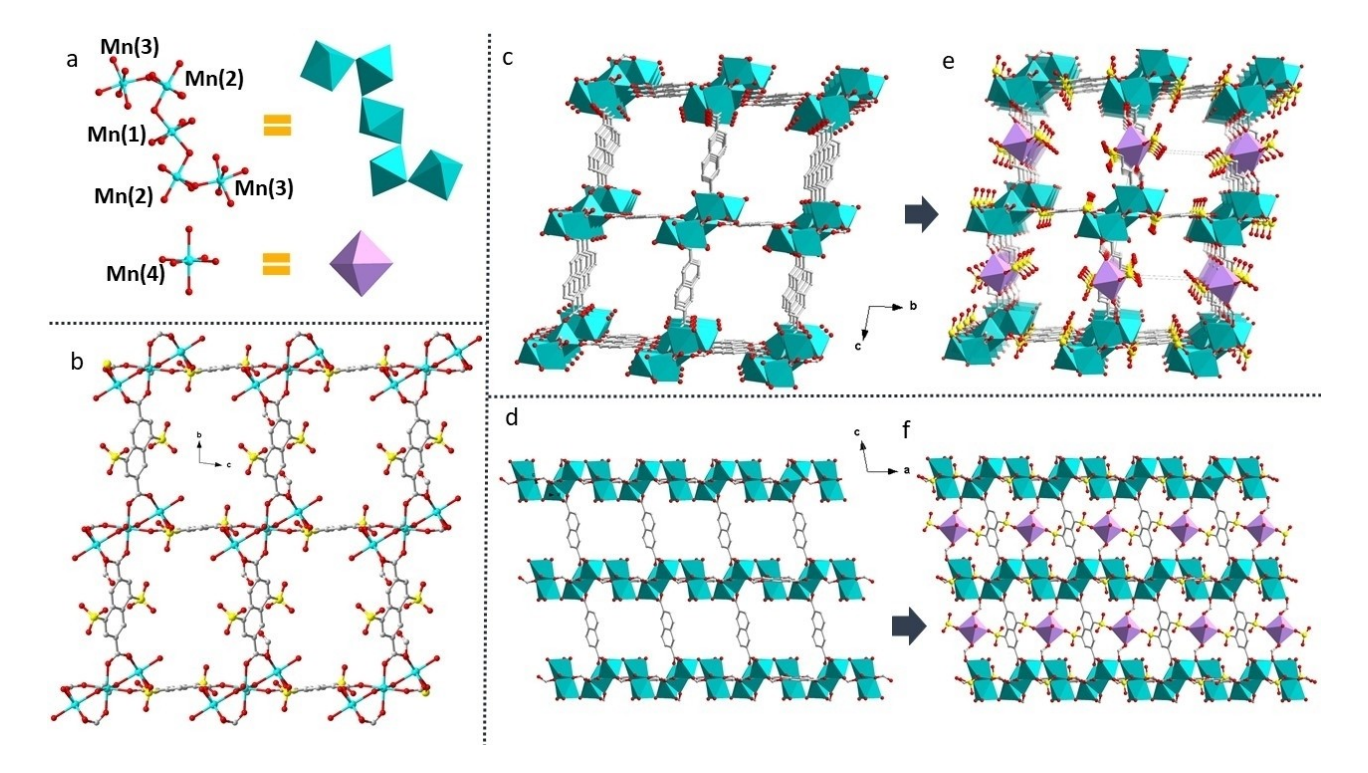


Figure 2. Graphic representations of CPM-s7. a) octahedrally coordinated Mn²⁺ chain and monomeric Mn²⁺ building unit, b) Expansion of Mn(1) and Mn(2) into 2D square layer, c-f) layers connected by Mn(3) and Mn(4) and sulfonate groups into 3D framework with 1D channel. In c-d) pendant groups and Mn(4) are removed for clarity. All non-bonding water molecules are also removed from drawings.

Chemistry Europe

European Chemical Societies Publishing

distance ranges from 2.063(9) to 2.240(8) Å (Figure S3). Each pair of (μ_3 -OH) bridge two sets of three Co atoms into a crossshaped pentamer (Figure 3a). The adjacent Co-Co distance within the pentamer ranges from 3.241(7) to 3.516(6) Å. For each (μ_3 -OH) bridged metal trimer, SO_4^{2-} further caps from above or below $M_3(\mu_3\text{-OH})$ plane. These pentamers are linked into 1D zigzag chains with HCOO⁻ ions. These zigzag chains are further linked by both sulfonate and carboxylate functional groups of dsndc⁴⁻ into 2D layers (Figure 3c). The neighboring layers are parallel to each other, with the shortest interlayer distance of 4.1 Å (O-O distances between two capping sulfates).

The in situ formation of sulfate capping agent resulted in more symmetrical metal oxide chains. In CPM-s7, the manganese oxide chain exhibits 2 corner-sharing MnO₆ octahedra (Mn(1)-O-Mn(2), 3.746 Å (M-M), and Mn(2)-O-Mn(3), 3.740 Å (M-M)), and one edge-sharing MnO₆ (Mn(3)-O-Mn(3), 3.674 Å (M—M)). In comparison, cobalt oxide chain of CPM-s8 shows one corner-sharing CoO₆ (Co(1)–O–(Co(3), 3.480 Å (M–M)), and two edge sharing CoO₆ (Co(1)-O-Co(2), 3.242 Å (M-M), and Co-(2)–O–Co(2), 3.393 Å (M–M)). The increase of edge-sharing octahedra in CPM-s8 leads to flattening of the metal chain, and could thus allow for better orbital overlap, which is highly beneficial in fabricating magnetic materials.

PXRD and Thermal Analysis: The phase purity of CPM-s8 was determined through powder X-ray diffraction (Figure S4). Assynthesized material matches well with simulated patterns from single-crystal data, suggesting high purity of bulk material. Thermal stability of CPM-s8 was further analyzed through thermogravimetric analysis (TGA) measurement under N₂ atmosphere (Figure S5). Initial 21% weight loss before 200°C correspond to solvent molecules in the pore. The second weight loss at 250 °C represent decomposition of organic linker and collapse of framework.

Magnetization Characterization: Of particular interest is the potential ordered-alignment of unpaired electrons in zigzag cobalt-oxide chains of CPM-s8. More interestingly, the number of unique crystallographic positions of cobalt is an odd number, thus preventing complete cancelling of antiparallel spins, such as in the case of antiferromagnetic materials. To better understand magnetic property of CPM-s8, we recorded temperaturedependent magnetization data under zero-field-cooling (ZFC) and field-cooling (FC) processes at magnetic field of 100 and 1000 Oe, between 2 and 350 K (Figures 4 and S5). As shown in Figure 4 (inset), the FC plot (at 1000 Oe) could be fitted by the Curie-Weiss equation, leading to Curie and Weiss constants of C=8.75 emu Oe⁻¹ K per formula unit [5 cobalt(II) ions] and θ = -21 K, respectively (Figure 4a, inset). The effective magnetic moment per cobalt(II) as estimated from the Curie constant is ~1.67 μ_B , indicative of low-spin cobalt(II) ions (~1.73 μ_B). A negative θ value suggests dominating antiferromagnetic interactions among the cobalt(II) centers. Indeed, the ZFC curve at 100 Oe (Figure 4) shows a peak at 8 K, further confirming the presence of antiferromagnetic (AFM) interactions. However, application of a small magnetic field, as the FC curve shows (Figure 4), destroys this peak, thus suggesting that the more likely magnetic ordering is ferrimagnetic with a $T_{\rm C}$ = 8 K. Indeed, the field-dependent magnetization data clearly shows a hyste-

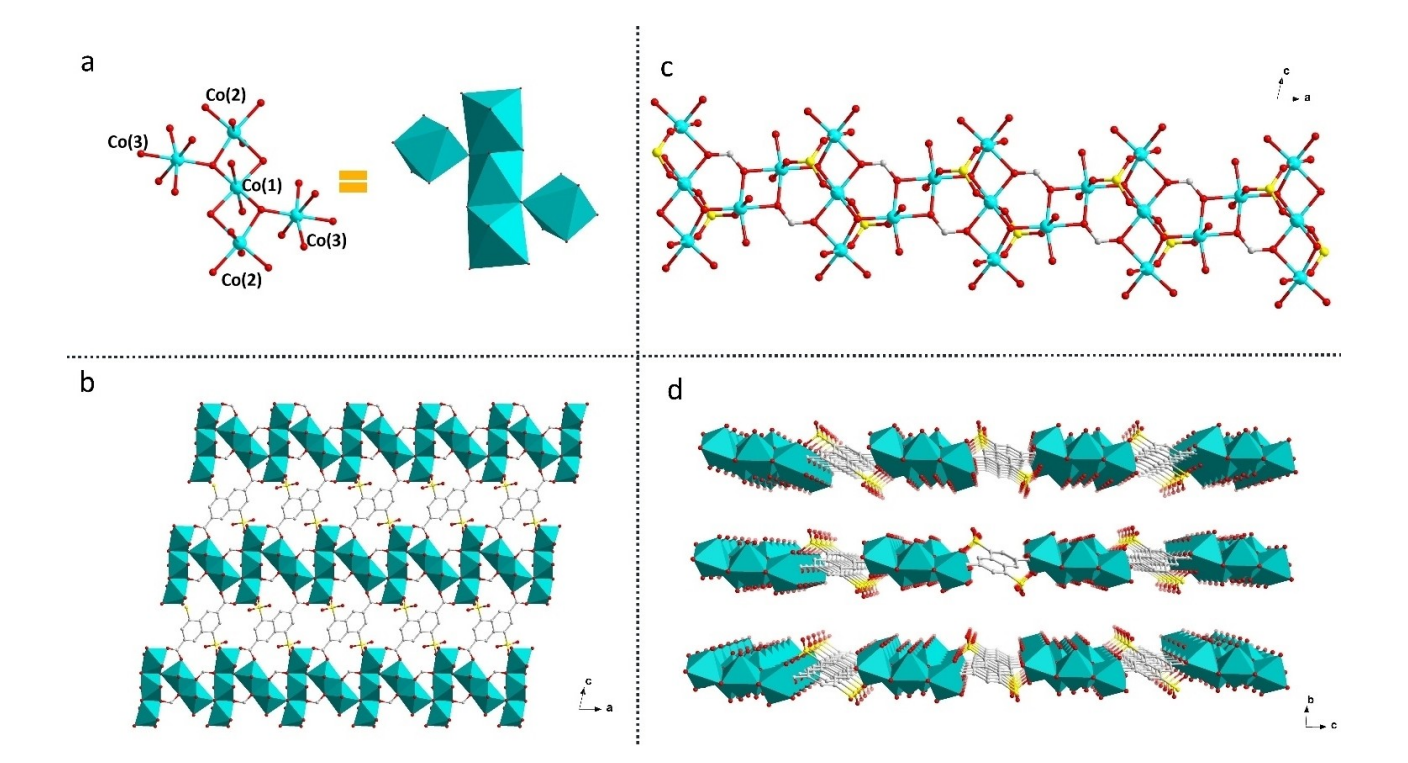


Figure 3. Graphic representations of CPM-s8. (a) octahedrally coordinated cobalt pentamer, with Co(1) residing on symmetry equivalent site, (b) 1D cobalt chain with bridging hydroxide, sulfate, and formate linkers, (c) 2D sheet in ac-plane, (d) View of parallelly stacked 2D layers in bc-plane.

Chemistry Europe

European Chemical Societies Publishing

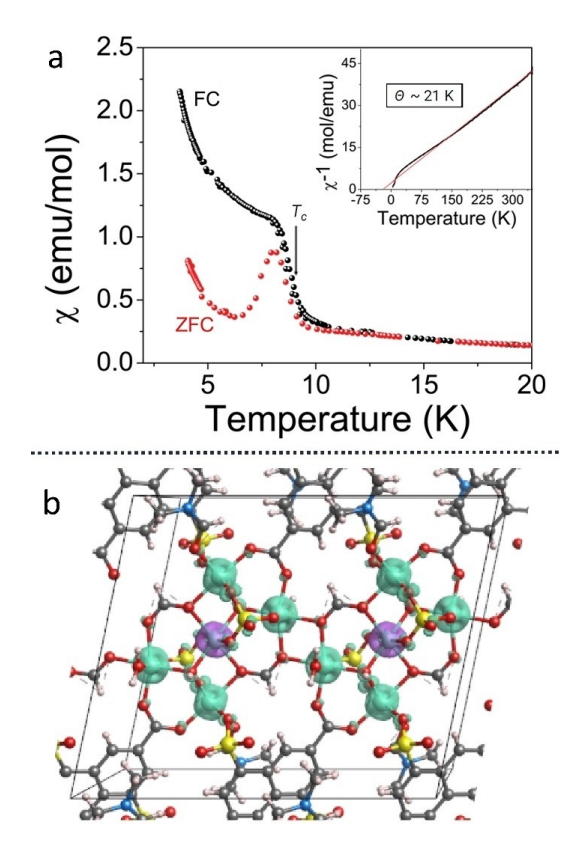


Figure 4. (a) Temperature-dependent ZFC and FC molar susceptibility curve of CPM-s8 recorded at 100 Oe. Inset shows the FC inverse molar susceptibility curve (at 1000 Oe) and the Curie-Weiss straight line (red). (b) DFT predicted ground state spin density distribution in a $2 \times 1 \times 1$ supercell of CPM-s8

resis at 5 K (Figure s7), albeit with very small remanence and saturation was not reached at the maximum magnetic field applied (40 kOe). Density functional theory calculations using the Hubbard onsite potential (DFT+U) have suggested that the ground state spin ordering is ferrimagnetic model with Co(2) and Co(3) in the spin-up configuration while the central Co(1) is spin-down, as shown in the spin density map in Figure 4b. This spin arrangement is dominated by AFM interactions (4) versus only 2 FM (ferromagnetic) ones, and a net magnetic moment will result. Furthermore, this pentameric unit is composed of 2 triangles, suggesting that geometric frustration would be possible if the triangles were equilateral. However, the different distances within the triangles eliminate (or strongly reduce) the frustration.

Conclusion

Based on structural analysis of newly synthesized 3D rod-packing manganese-based framework, strategic design of capping agent was developed to obtain a 2D rod-packing framework. SQUID measurements and DFT calculations proved ferrimagnetic ordering of the material below 8 K, further illustrating the potential of developing spintronic materials through 2D rod-packing MOFs.

Experimental Section

All starting materials and solvents were commercially available and used without further purification.

Synthesis of 4,8-disulfo-napthalene-2,6-dicarboxylic acid (H_4 dsndc): H_4 dsndc was synthesized according to reported literature with slight modification. (P) Naphthalene-2,6-dicarboxylic acid (7 g) was added to 25 mL of oleum (SO_3 , 30 wt %) in a 100 mL round-bottom flask equipped with reflux condenser. The reaction mixture was stirred vigorously at 150 °C for 6 h. Solution mixture was dissolved in distilled water, followed by precipitation in HCl (36 wt%). Isolated product was washed with ice-water to removed trapped HCl and dried in vacuum over at 120 °C overnight. Yield (85 %), 1 H NMR (600 MHz, DMSO-d₆ δ , ppm): 8.5 (d), 9.6 (d).

Synthesis of CPM-s7: In a 23 mL glass vial, MnCl $_2\cdot$ 4H $_2$ O (70 mg, \sim 0.3 mmol), H $_4$ dsndc (40 mg, 0.1 mmol) were dissolved in 4.0 g N,N-dimethylformamide (DMF), 4.5 g ethanol (EtOH) and 4.0 g deionized water (DI H $_2$ O). After stirring for 1 h, the vial was placed in a 120 °C oven for 7 days. Clear spindle-shaped crystals are obtained after solution was cooled to ambient temperature. Yield 50% based on H $_4$ dsndc.

Synthesis of CPM-s8: In a 23 mL glass vial, $CoCl_2 \cdot 6H_2O$ (76 mg, 0.3 mmol), H_4 dsndc (40 mg, 0.1 mmol) were dissolved in 4.0 g DMF, 4.5 EtOH and 4.0 g DI H_2O . After stirring for 1 h, the vial was placed in a 120 °C oven for 7 days. Pink spindle-shaped crystals are obtained after solution was cooled to ambient temperature. Yield 30% based on H_4 dsndc.

Single-Crystal X-ray Diffraction (SXRD) Characterization: The single-crystal X-ray diffraction measurements were performed on a Bruker diffractometer using graphite-monochromated MoK α (λ = 0.71073 Å) radiation at room temperature. Diffraction data were integrated and scaled by 'multi-scan' method with the Bruker APEX software. The structure was solved by direct methods and refined using SHELXTL. [10] SQUEEZE routine in PLATON software package was employed to fix solvents in lattice pores. [11] Crystal data, as well as details of data collection and refinements, are summarized in Table S1–S2. Deposition Numbers 2174006 (for CPM-s7) and 2174007 (for CPM-s8) contain the supplementary crystallographic data for this paper. These data are provided free of charge by the joint Cambridge Crystallographic Data Centre and Fachinformationszentrum Karlsruhe Access Structures service.

Powder X-ray Diffraction (PXRD) Characterization: Powder X-ray diffraction experiments were performed on a PANalytical Empyrean Series 2 with CuK α radiation (40 kV, 40 mA, λ =1.5418 Å). Mercury 4.3.0 is used to simulate powder pattern from single crystal data.

Thermal-gravimetric Analysis: TA Instruments TGA Q500 thermal analyzer was used to measure the thermogravimetric (TG) curve at heating rate of 5 °C/min under nitrogen flow at 60 mL per minute.

Magnetization Measurement: The magnetization measurements were performed on a physical properties measurement system (PPMS) equipped with a superconducting quantum interference device (SQUID). The zero field and field cooled measurements were performed under magnetic fields of 100 and 1000 Oe. Hysteresis loops were measured between -40000 Oe and 40000 Oe at 5 K. The data were corrected for the sample holder (Teflon tubes). The molar mass used for data analysis was that of the solvent-filled CMP-s8.

DFT Calculations: DFT+U calculations were performed using projector augmented wave pseudo potentials to model core electrons with the Perdew-Burke-Ernzerhof exchange correlation functional.^[12] Brillouin zone integration was performed using a 3x3x3 k-point mesh. Starting from structures obtained from XRD,

Europe European Chemical Societies Publishing

Chemistry

structures were relaxed to minimize energy with a tolerance of 10^{-6} eV. The calculations were performed using a U energy of 3.2 eV, but the same qualitative magnetic ordering was found to persist in calculations using U values between 0 and 5 eV.

Acknowledgements

We acknowledge the support of this work by the US Department of Energy, Office of Basic Energy Sciences, Materials Sciences and Engineering Division under Award No. DE-SC0010596 (P.F.).

Conflict of Interest

The authors declare no conflict of interest.

Data Availability Statement

The data that support the findings of this study are available from the corresponding author upon reasonable request.

Keywords: density functional calculations properties · metal-organic frameworks · metal rods · sulfonate linkers

- [1] a) H. Jiang, D. Alezi, M. Eddaoudi, Nat. Rev. Mater. 2021, 6, 466-487; b) R. Freund, S. Canossa, S. M. Cohen, W. Yan, H. Deng, V. Guillerm, M. Eddaoudi, D. G. Madden, D. Fairen-Jimenez, H. Lyu, L. K. Macreadie, Z. Ji, Y. Zhang, B. Wang, F. Haase, C. Wöll, O. Zaremba, J. Andreo, S. Wuttke, C. S. Diercks, Angew. Chem. Int. Ed. 2021, 60, 23946-23974; c) N. Behera, J. Duan, W. Jin, S. Kitagawa, EnergyChem 2021, 3, 100067.
- [2] a) M. J. Kalmutzki, N. Hanikel, O. M. Yaghi, Sci. Adv. 2018, 4, eaat9180; b) H. Furukawa, K. E. Cordova, M. O'Keeffe, O. M. Yaghi, Science 2013, 341, 1230444.
- [3] a) N. L. Rosi, J. Kim, M. Eddaoudi, B. Chen, M. O'Keeffe, O. M. Yaghi, J. Am. Chem. Soc. 2005, 127, 1504-1518; b) A. Schoedel, M. Li, D. Li, M. O'Keeffe, O. M. Yaghi, Chem. Rev. 2016, 116, 12466-12535; c) X. Zhao, M. S. Shimazu, X. Chen, X. Bu, P. Feng, Angew. Chem. Int. Ed. 2018, 57, 6208-6211; Angew. Chem. 2018, 130, 6316-6319; d) H. Yang, F. Peng, C.

- Dang, Y. Wang, D. Hu, X. Zhao, P. Feng, X. Bu, J. Am. Chem. Soc. 2019, 141, 9808-9812; e) F. Peng, H. Yang, A. Hernandez, D. E. Schier, P. Feng, X. Bu, Chem. Eur. J. 2020, 26, 11146-11149.
- [4] L. J. Wang, H. Deng, H. Furukawa, F. Gandara, K. E. Cordova, D. Peri, O. M. Yaghi, Inorg. Chem. 2014, 53, 5881-5883.
- [5] B. Li, H.-M. Wen, H. Wang, H. Wu, T. Yildirim, W. Zhou, B. Chen, Energy Environ. Sci. 2015, 8, 2504-2511.
- [6] L. Sun, C. H. Hendon, M. A. Minier, A. Walsh, M. Dincă, J. Am. Chem. Soc. 2015. 137. 6164-6167.
- [7] a) X. Wang, B. Li, Y.-P. Wu, A. Tsamis, H.-G. Yu, S. Liu, J. Zhao, Y.-S. Li, D.-S. Li, Inorg. Chem. 2020, 59, 4764-4771; b) E. J. Kim, R. L. Siegelman, H. Z. H. Jiang, A. C. Forse, J.-H. Lee, J. D. Martell, P. J. Milner, J. M. Falkowski, J. B. Neaton, J. A. Reimer, S. C. Weston, J. R. Long, Science 2020, 369, 392; c) L. Li, R.-B. Lin, R. Krishna, H. Li, S. Xiang, H. Wu, J. Li, W. Zhou, B. Chen, Science 2018, 362, 443-446; d) P. J. Milner, R. L. Siegelman, A. C. Forse, M. I. Gonzalez, T. Runčevski, J. D. Martell, J. A. Reimer, J. R. Long, J. Am. Chem. Soc. 2017, 139, 13541-13553; e) S. J. Geier, J. A. Mason, E. D. Bloch, W. L. Queen, M. R. Hudson, C. M. Brown, J. R. Long, Chem. Sci. 2013, 4, 2054-2061; f) Y. S. Bae, C. Y. Lee, K. C. Kim, O. K. Farha, P. Nickias, J. T. Hupp, S. T. Nguyen, R. Q. Snurr, Angew. Chem. Int. Ed. Engl. 2012, 51, 1857-1860; g) Z. Bao, J. Wang, Z. Zhang, H. Xing, Q. Yang, Y. Yang, H. Wu, R. Krishna, W. Zhou, B. Chen, Q. Ren, Angew. Chem. Int. Ed. Engl. 2018, 57, 16020-16025; h) D. E. Jaramillo, H. Z. H. Jiang, H. A. Evans, R. Chakraborty, H. Furukawa, C. M. Brown, M. Head-Gordon, J. R. Long, J. Am. Chem. Soc. 2021, 143, 6248-6256; i) A. Shigematsu, T. Yamada, H. Kitagawa, J. Am. Chem. Soc. 2011, 133, 2034-
- [8] a) M. Wang, X. Gou, W. Shi, P. Cheng, Chem. Commun. (Camb.) 2019, 55, 11000-11012; b) X.-B. Li, J.-Y. Zhang, Y.-Q. Wang, Y. Song, E.-Q. Gao, Chem. Eur. J. 2011, 17, 13883-13891; c) Y.-Z. Zheng, M.-L. Tong, W.-X. Zhang, X.-M. Chen, Angew. Chem. Int. Ed. 2006, 45, 6310-6314; Angew. Chem. 2006, 118, 6458-6462; d) S. Hu, L. Yun, Y.-Z. Zheng, Y.-H. Lan, A. K. Powell, M.-L. Tong, Dalton Trans. 2009, 1897–1900; e) B.-W. Hu, J.-P. Zhao, Q. Yang, X.-F. Zhang, M. Evangelisti, E. C. Sañudo, X.-H. Bu, Dalton Trans. 2010, 39, 11210-11217; f) Z.-X. Li, Y.-F. Zeng, H. Ma, X.-H. Bu, Chem. Commun. 2010, 46, 8540-8542; g) S.-Y. Zhang, W. Shi, Y. Lan, N. Xu, X.-Q. Zhao, A. K. Powell, B. Zhao, P. Cheng, D.-Z. Liao, S.-P. Yan, Chem. Commun. 2011, 47, 2859-2861; h) Y.-Q. Wang, A.-L. Cheng, P.-P. Liu, E.-Q. Gao, Chem. Commun. 2013, 49, 6995-6997; i) A. Kawamura, A. S. Filatov, J. S. Anderson, I.-R. Jeon, Inorg. Chem. 2019, 58, 3764-3773.
- [9] Q.-Y. Liu, W.-F. Wang, Y.-L. Wang, Z.-M. Shan, M.-S. Wang, J. Tang, Inorg. Chem. 2012, 51, 2381-2392.
- [10] G. Sheldrick, Acta Crystallogr. Sect. A 2008, 64, 112-122.
- [11] A. Spek, J. Appl. Crystallogr. 2003, 36, 7–13.
- [12] J. P. Perdew, K. Burke, M. Ernzerhof, Phys. Rev. Lett. 1996, 77, 3865-3868.

Manuscript received: May 20, 2022 Accepted manuscript online: June 22, 2022 Version of record online: July 25, 2022